Journal of Power Sources 196 (2011) 851–854

Contents lists available at ScienceDirect

Journal of Power Sources

journal homepage: www.elsevier.com/locate/jpowsour

Short communication

Characterization of $MnFe_2O_4$/$LiMn_2O_4$ aqueous asymmetric supercapacitor

Yen-Po Lin, Nae-Lih Wu*

Department of Chemical Engineering, National Taiwan University, Taipei 106, Taiwan

ARTICLE INFO

Article history:
Received 14 May 2010
Received in revised form 9 July 2010
Accepted 21 July 2010
Available online 1 August 2010

Keywords:
Asymmetric supercapacitor
Manganese ferrite
Lithium manganese oxide
Specific energy
Self-discharge

ABSTRACT

A new type of asymmetric supercapacitor containing a $MnFe_2O_4$ negative electrode and a $LiMn_2O_4$ positive electrode in aqueous $LiNO_3$ electrolyte has been synthesized and characterized. The nanocrystalline $MnFe_2O_4$ anode material has a specific capacitance of 99 F g^{-1} and the $LiMn_2O_4$ cathode a specific capacity of 130–100 mAh g^{-1} under 10–100 C rate. The cell has a maximum operating voltage window of ca. 1.3 V, limited by irreversible reaction of $MnFe_2O_4$ toward reducing potential. The specific power and specific energy of the full-cell increase with increasing anode-to-cathode mass ratio (A/C) and saturate at A/C ~4.0, which gives specific cell energies, based on total mass of the two electrodes, of 10 and 5.5 Wh kg^{-1} at 0.3 and 1.8 kW kg^{-1}, respectively. The cell shows good cycling stability and exhibits significantly slower self-discharge rate than either the $MnFe_2O_4$ symmetric cell or the other asymmetric cells having the same cathode but different anode materials, including activated carbon fiber and MnO_2.

1. Introduction

Asymmetric supercapacitors are promising energy storage devices, being capable of charging/discharging faster than batteries and having higher energy densities than traditional electric double-layer capacitors (EDLCs). Based on the electrochemical properties of the electrode materials, they can in general be divided into two major categories. The first kind of asymmetric supercapacitors contains two electrodes of different materials exhibiting capacitive behavior over different potential ranges so that the overall operation voltage window of the cell can be enlarged and its energy density becomes greater than the symmetric cells containing solely either kind of the electrodes [1–3]. The second type combines a battery electrode with a capacitor electrode in one cell [4–6]. As the battery electrode charges/discharges at a plateau potential, the cell is capable of storing a greater amount of energy than the symmetric cell of the capacitive electrodes even within the same operating voltage window. Most of the existing examples of this category [5,6], such as activated carbon (AC)/PbO_2 and AC/NiO, employ an EDLC material for the capacitor electrode. The only cell, to our knowledge, that uses pseudocapacitve material for this purpose is MnO_2/$LiMn_2O_4$ [7] with a Li^+-containing organic electrolyte. However, the cell was not tested for cycle-life and self-discharge characteristics.

Nanocrystalline $MnFe_2O_4$ is a pseudocapacitive material possesses high-power delivering capability [8–10]. In contrast to MnO_2-based pseudocapacitive materials, which are essentially amorphous, $MnFe_2O_4$ exhibits pseudocapacitance in crystalline form, and its symmetric cell has been shown to exhibit superior cycling stability than the amorphous-MnO_2 ones in aqueous electrolytes [9]. In this work, a new type of asymmetric supercapacitor which consists of a $MnFe_2O_4$-carbon black composite, abbreviated as $MnFe_2O_4$@C, anode and a $LiMn_2O_4$ cathode has been synthesized and characterized for its fundamental operating characteristics, including energy and power capabilities, cycling stability and self-discharge behavior.

2. Experimental

The preparation procedure for the $MnFe_2O_4$@C composite powder, which has an oxide-to-carbon mass ratio of 74:26, has been described in detail elsewhere [8,9]. In brief, aqueous solution containing $MnSO_4$ and $FeCl_3$ (Mn^{2+}:Fe^{3+} = 1:2) and predetermined amount of carbon black powder was simultaneously introduced into a 1.5 M $NaOH_{(aq)}$ solution under vigorous stirring. Black precipitate formed immediately upon mixing, and was subsequently washed with de-ionized water to remove residual anions. Finally, the powder was dried in air at 50 °C, followed by calcination at 350 °C in N_2 for 2 h. $LiMn_2O_4$ was a courtesy from Industrial Technology Research Institute, Taiwan.

The cathode electrode contained 63 wt% $LiMn_2O_4$, 25 wt% KS6 (Timcal), 5 wt% Super P (Timcal) and 7 wt% polyvinylidene fluoride (PVdF, Aldrich), while the anode contained 93 wt% $MnFe_2O_4$@C and 7 wt% PVdF. Both electrodes used Ti foil as current collector, and the active-layers were prepared by a slurry-casting method using N-methylpyrrolidone (NMP; Mitsubishi Chemical) as solvent. The electrodes were finally dried at 120 °C in an oven for 6 h.

* Corresponding author. Tel.: +886 2 23627158; fax: +886 2 23623040.
E-mail address: nlw001@ntu.edu.tw (N.-L. Wu).

0378-7753/$ – see front matter © 2010 Elsevier B.V. All rights reserved.
doi:10.1016/j.jpowsour.2010.07.066

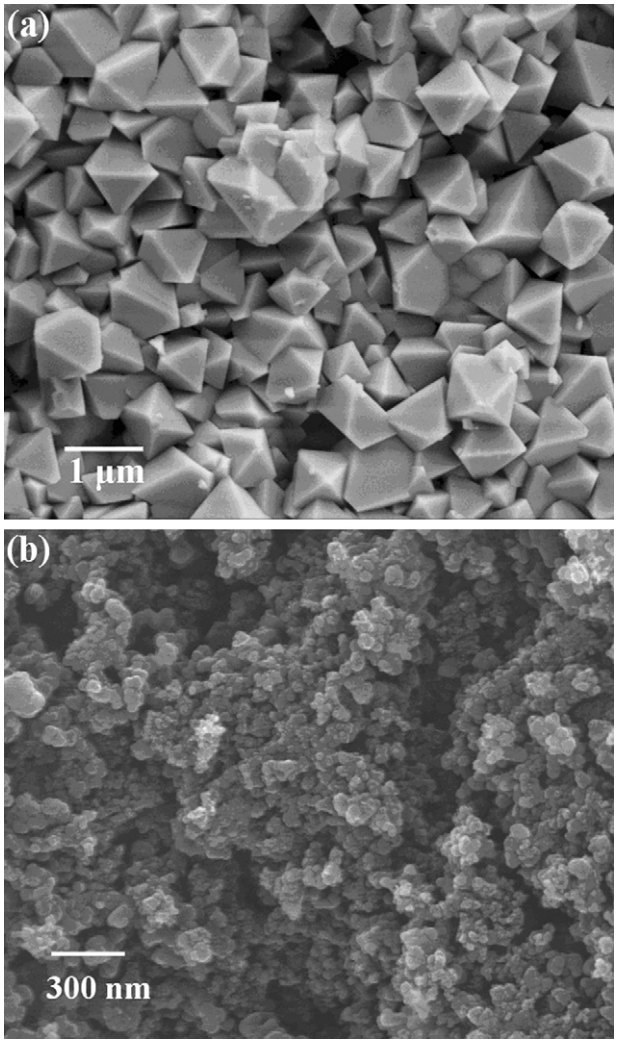

Fig. 1. SEM micrographs of (a) $LiMn_2O_4$ and (b) $MnFe_2O_4$@C composite.

Full-cells were assembled with the two electrodes face-to-face and a porous separator (BS0712, Coin Nano Tech) in between. The measurements were typically carried out with the cells immersed in excess amount of electrolyte, except for the cycling-stability studies, where the cells were removed from the electrolyte container and tested in an empty sealed container. All electrochemical analyses were conducted on an electrochemical analyzer (CHI 405a, CH Instrument). The three-electrode configuration, which consisted of a Pt counter electrode, a Ag/AgCl/saturated $KCl_{(aq)}$ (EG&G, potential is 197 mV versus NHE at 25 °C) reference electrode and a working electrode, was employed to characterize the electrochemical behaviors of individual electrodes. The potentials mentioned hereafter are based on this reference electrode. The two-electrode configuration, however, was adopted for the full-cell characterization. In some full-cell experiments, the potential of each of the electrodes were independently monitored against a reference electrode.

3. Results and discussion

3.1. Individual materials and electrodes

The spinel $LiMn_2O_4$ crystallites have an octahedral shape with a rather uniform particle size close to 1.0 μm (Fig. 1a). In contrast, the $MnFe_2O_4$@C powder contains rounded particles with sizes no

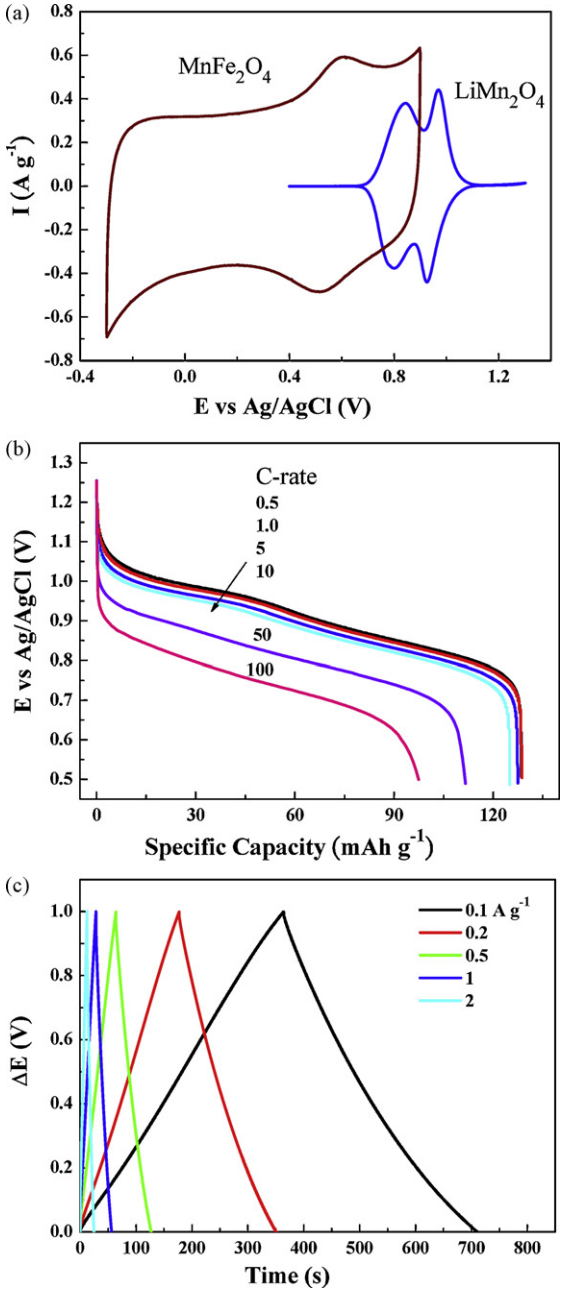

Fig. 2. Electrochemical characterization of individual electrodes: (a) voltammograms of $MnFe_2O_4$@C anode (4 mV s^{-1}) and $LiMn_2O_4$ cathode (0.2 mV s^{-1}); (b) galvanostatic discharge potential curves of $LiMn_2O_4$ cathode; (c) galvanostatic charge/discharge voltage curves of the $MnFe_2O_4$ symmetric cell (the current densities are based on the mass of $MnFe_2O_4$@C in one electrode.).

greater than a few tens nanometers (Fig. 1b). The average crystal size of $MnFe_2O_4$, as determined from the line-broadening of X-ray diffraction peak, is 13 nm, while the N_2-adsorption BET surface area is 160 $m^2\ g^{-1}$.

Fig. 2a compares the voltammograms of the individual electrodes. $MnFe_2O_4$@C anode showed reversible capacitive behavior within −0.3 and 0.9 V. Irreversible reduction of the oxide electrode becomes significant below −0.3 V, while irreversible oxidation starts to occur above 0.9 V. A pair of redox humps centered at ~0.6 V results mainly from charge transfer at the Fe-ion sites [10], while the charge transfer at the Mn-ion sites occurs throughout the entire potential range. The capacitance of the $MnFe_2O_4$@C composite is 69 F g^{-1} at 4 mV s^{-1}. As the specific capacitance of the carbon

Table 1
Properties of individual electrodes of $MnFe_2O_4$ (anode)/$LiMn_2O_4$ (cathode) cells.

Sample name	Geometric AM[a] density (mg cm^{-2})		Operating specific capacity[b] (mAh g^{-1}-AM[a])		Specific cell capacity[c] (mAh g^{-1}-total)	Capacity retention after 5000 cycles (%)
	Anode	Cathode	Anode	Cathode		
1-1	0.69	0.67	29.9	30.8	10.0	94
2-1	1.47	0.67	31.6	69.2	13.9	95
3-1	1.66	0.67	30.5	73.9	14.6	94
4-1	2.35	0.67	32.6	115	16.5	90

[a] AM: the oxide active–materials (not including carbon).
[b] Specific capacities of the active materials measured at the lowest current rates shown in Fig. 4a.
[c] Specific capacity of the cell based on the total mass of the active-layers (including binder) on two electrodes at the lowest current rate shown in Fig. 4a.

black, as determined from its pure electrode, is ~5 F g^{-1}, the specific capacitance of the $MnFe_2O_4$ component is thus estimated to be ca. 99 F g^{-1}.

The voltammogram of the $LiMn_2O_4$ electrode shows two redox pairs. One pair is located at 0.85 V, while the other located at 0.95 V. They correspond to the lithiation and de-lithiation reactions of $Li_xMn_2O_4$ with $0.5 \le x \le 1$ and $0 \le x \le 0.5$, respectively. The potential difference between the oxidation and reduction peaks is very small, indicating high reversibility. From Fig. 2a, it can be seen that this asymmetric system has a maximum operating voltage window of ca. 1.3 V.

Fig. 2b shows the potential curves of the cathode at different C-rates. (The C-rate is calculated based on the theoretical specific capacity of 148 mAh g^{-1} for $LiMn_2O_4$.) It was found that the specific capacity is 128 mAh g^{-1} at 0.5 C rate, and it does not decreases much, by less than 5%, as the current is increased to 10 C rate (1.48 A g^{-1}). The cathode remains capable of delivering a capacity of 97 mAh g^{-1} at 100 C-rate (14.8 A g^{-1}). The coulombic efficiencies are all greater than 99%. The contribution to the overall capacity due to the capacitance of the conductive additives (0.69 mAh g^{-1} or 2.5 F g^{-1}) is negligible. Fig. 2C shows the galvanostatic charge/discharge voltage curves of a $MnFe_2O_4$ symmetric cell under different current densities. They all show linear correlation between voltage and discharge time, typical of a capacitor.

3.2. Full-cell characterization

Three full-cells having different anode-to-cathode (A/C) mass ratios, including those close to 1:1, 2:1, 3:1 and 4:1, were characterized (Table 1). These cells have the same active-material loading (g cm^{-2}) on cathode but varied loadings on anode. For brevity, these cells will hereafter be referred to as the 1-1, 2-1, 3-1 and 4-1 cells, respectively. Galvanostatic charge/discharge tests of the full cells give linear voltage curves (Fig. 3). The inset in Fig. 3 shows an example of the potential plots of individual electrodes during the test, confirming the battery and capacitor behaviors for cathode and anode, respectively, during the full-cell operation.

The power and energy performances among these cells are illustrated in two ways. Fig. 4a plots the specific cell capacitance and capacity, both based on the total mass of the active-layers (including binder) versus current density and C-rates. As the cathode side is likely the limiting electrode for power performance, all the current data are calculated based on the cathode active-material loading (the *x*-axis). The operating specific capacities for individual electrodes at their lowest tested current rates are listed in Table 1. Data

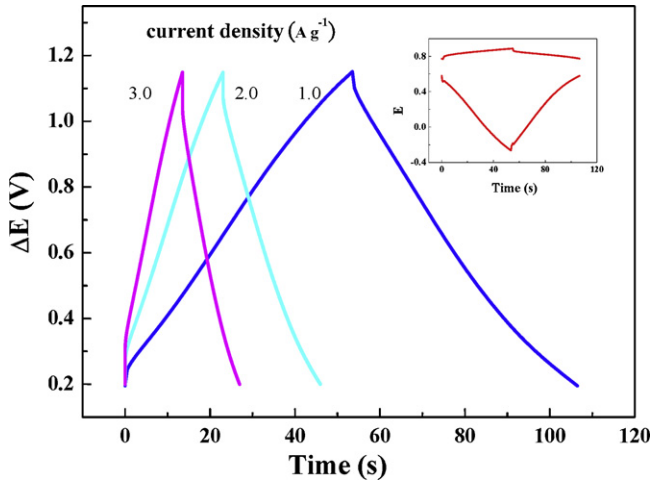

Fig. 3. Galvanostatic charge/discharge voltages curves of $MnFe_2O_4$@C/$LiMn_2O_4$ full-cell (inset: potential curves of $MnFe_2O_4$@C anode and $LiMn_2O_4$ for current density of 1 A g^{-1}).

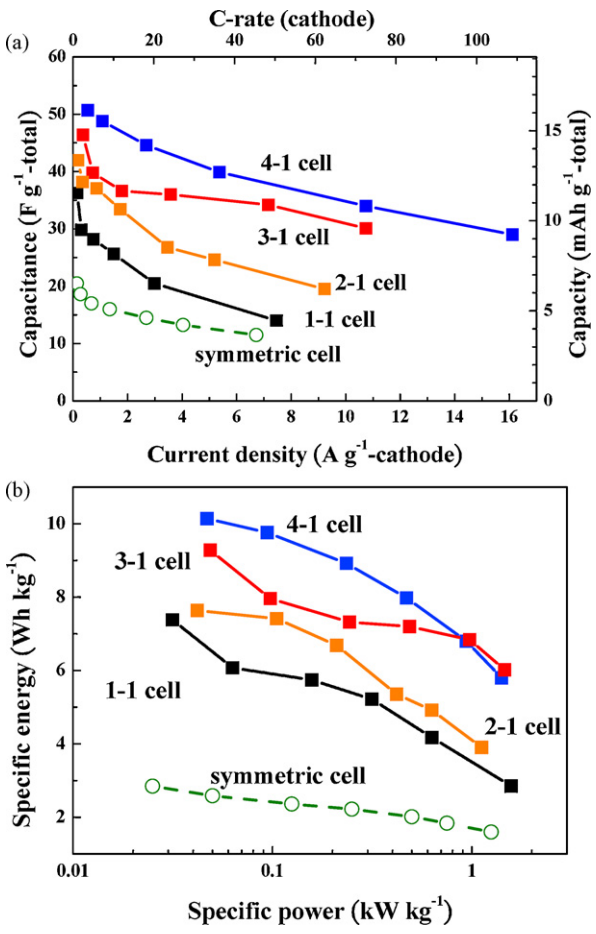

Fig. 4. Energy and power performance of $MnFe_2O_4$@C/$LiMn_2O_4$ full-cells having different anode-to-cathode mass ratios: (a) specific cell capacitance and capacity, based on total active-layer mass on two electrodes, versus current density/C-rate of cathode; (b) Ragone plot showing specific cell energy versus specific cell power.

from a symmetric $MnFe_2O_4$ cell, which has an operating voltage window of 1.0 V [8], are also shown for comparison.

It is clearly shown (Fig. 4a) that all the asymmetric cells have higher cell capacitances/capacities than the symmetric cell. When one of the $MnFe_2O_4$ electrodes in the symmetric cell was replaced with a $LiMn_2O_4$ electrode of equal mass (the 1-1 cell), the cell specific capacitance increases by nearly 50%. With further increase in the A/C ratio, the specific cell capacitance further increases and saturates at A/C ~4. On the other hand, the capacitances/capacities of the asymmetric cells are more sensitive to the current rate, decreasing by greater extents with increasing current rate, as compared with the symmetric cell. Nevertheless, the asymmetric cells remain having much higher capacities than the symmetric cell over a wide range of current rate.

Fig. 4b illustrates the power and energy performances of the cells in a Ragone plot. The specific energy E and specific power P are calculated from

$$E = (1/2)C V_u^2$$
$$P = (1/2)I V_u$$

where C is the specific cell capacitance, V_u is the adopted upper end of the operating voltage window (1.2 V), and I is the current density based on the total mass of the active-layers. The 4-1 cell, which has the highest energy capacity among all the cells, exhibits a saturated specific energy of ca. 10 Wh kg^{-1} toward low-power end and a specific energy of 5.5 Wh kg^{-1} at 1.8 kW kg^{-1}. The former is comparable with that of AC/NiO but lower than that of either AC/$LiMn_2O_4$ or AC/PbO_2 (ca. 25 Wh kg^{-1}) aqueous supercapacitor [11]. The main limiting factor for energy storage of the present system resides in the irreversible reaction of $MnFe_2O_4$ toward reducing potential, as shown in Fig. 2a, which severely limits the allowable operating voltage window. The operating voltage window of either AC/$LiMn_2O_4$ or AC/PbO_2, for example, was reported to be nearly 2.0 V, as contrast to the maximum voltage window of 1.3 V for the present system.

As mentioned earlier, the cycling-stability test was conducted by placing the wetted full-cell units in an empty chamber (i.e., without excess electrolyte). With this approach, any severe consumption of electrolyte due to undesired redox reaction (such as electrolysis) can easily be noted from the cell performance. As shown in Table 1, the asymmetric cells showed rather good cycling stability, exhibiting less than 10% capacity loss after 5000 cycles upon cycling up to 1.2 V at the current density of 1 A g^{-1}-anode. Examination of the capacities of individual electrodes after the cycling indicates that both cathode and anode suffer from certain extent of fading.

Comparison in self-discharge behavior of the cells of different combinations of electrode materials was performed by charging the representative cells up to 1 V and then opening the circuit while recording the variation in the cell voltage with time. As shown in Fig. 5, the asymmetric cell (the 4-1 cell) exhibits a much slower self-discharge rate than the symmetric cell. Moreover, it was found that the $MnFe_2O_4$/$LiMn_2O_4$ cell also self-discharges slower than another two types of asymmetric cells, namely AC fiber/$LiMn_2O_4$ and MnO_2/$LiMn_2O_4$, which have the same cathode as the present study but different anodes. For the asymmetric cells, the self-discharge rates basically follow the order of the self-discharge rates of the anode electrodes.

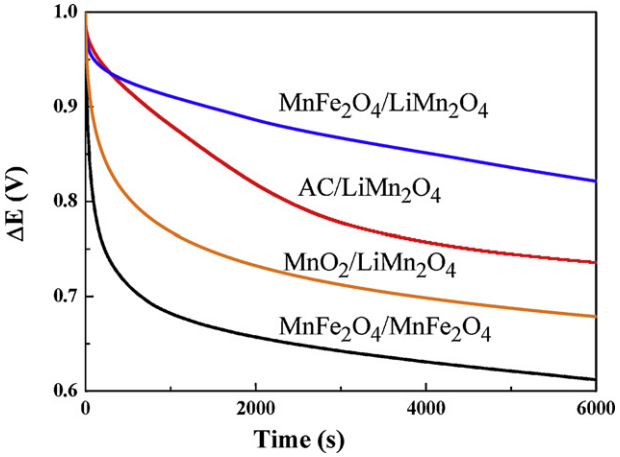

Fig. 5. Self-discharge voltage curves of $MnFe_2O_4$@C/$LiMn_2O_4$, MnO_2/$LiMn_2O_4$, activated carbon (AC) fiber/$LiMn_2O_4$ asymmetric cells and symmetric $MnFe_2O_4$@C cell.

Acknowledgements

The authors would like to thank the National Science Council of the Republic of China, Taiwan, for financially supporting this research under Contract No. NSC 98-3114-E-002-012 and NSC 98-3114-E-007-011.

References

[1] T. Brousse, D. Belanger, Electrochem. Solid-State Lett. 6 (2003) A244.
[2] M.S. Hong, S.H. Lee, S.W. Kim, Electrochem. Solid-State Lett. 5 (2002) A227.
[3] Y.G. Wang, Y.Y. Xia, Electrochim. Acta 50 (2005) 5641.
[4] G.G. Amatucci, F. Badway, A.D. Pasquier, T. Zheng, J. Electrochem. Soc. 148 (2001) A930.
[5] W.G. Pell, B.E. Conway, J. Power Sources 136 (2004) 334.
[6] Y.G. Wang, Y.Y. Xia, Electrochem. Commun. 7 (2005) 1138.
[7] S.B. Ma, K.W. Nam, W.S. Yoon, X.Q. Yang, K.Y. Ahn, K.H. Oh, K.B. Kim, Electrochem. Commun. 9 (2007) 2807.
[8] S.L. Kuo, N.L. Wu, Electrochem. Solid-State Lett. 8 (2005) A495.
[9] S.L. Kuo, N.L. Wu, J. Power Sources 162 (2006) 1437.
[10] S.L. Kuo, J.F. Lee, N.L. Wu, J. Electrochem. Soc. 154 (2007) A34.
[11] K. Naoi, P. Simon, Interface 17 (2008) 34.